DNS and LES of the Compressible Flow Over a Delta Wing With the Symmetry-Preserving Discretization

Rozema, Wybe; Kok, Johan C; Verstappen, Roel WCP; Veldman, Arthur EP

Published in:
ASME 2014 4th Joint US-European Fluids Engineering Division Summer Meeting collocated with the ASME 2014 12th International Conference on Nanochannels, Microchannels, and Minichannels

Proceedings of the ASME 2014 4th Joint US-European Fluids Engineering Division Summer Meeting and 11th International Conference on Nanochannels, Microchannels, and Minichannels
FEDSM2014
August 3-7, 2014, Chicago, Illinois, USA

FEDSM2014-21374

DNS AND LES OF THE COMPRESSIBLE FLOW OVER A DELTA WING WITH THE SYMMETRY-PRESERVING DISCRETIZATION

Wybe Rozema*
Johann Bernoulli Institute for
Mathematics and Computer Science
University of Groningen
Groningen, The Netherlands

Johan C. Kok
Aerospace Vehicles: Flight Physics & Loads
National Aerospace Laboratory NLR
Amsterdam, The Netherlands

Roel W. C. P. Verstappen and Arthur E. P. Veldman
Johann Bernoulli Institute for
Mathematics and Computer Science
University of Groningen
Groningen, The Netherlands

ABSTRACT

A fourth-order accurate symmetry-preserving discretization for compressible flow is used to perform simulations of the turbulent flow over a delta wing. A symmetry-preserving discretization eliminates the non-linear convective instability by preserving conservation of kinetic energy at the discrete level. This enhances the stability of a simulation method, so that little artificial dissipation is needed for numerical stability. It is shown that simulations of the flow over a sharp-edge delta wing at Re = 50,000 with the symmetry-preserving discretization are stable without artificial dissipation in a region of interest around the delta wing. To assess the accuracy of the simulation method, results obtained on a fine computational grid are compared with results obtained on a coarser grid. Also results obtained with large-eddy simulation models and with sixth-order artificial dissipation are presented.

*Corresponding author; w.rozema@rug.nl

INTRODUCTION

Preserving conservation laws in a numerical method can be advantageous for solving differential equations from fluid dynamics. The Lax-Wendroff theorem, for example, states that preserving conservation at the discrete level together with convergence implies convergence to an actual weak solution [1]. From a practical point of view, preserving mass conservation in a discretization prevents numerical leakage of a fluid, and preserving conservation laws at the discrete level is important for computing shock waves with an appropriate propagation speed. Naturally finite-volume methods, which are derived from the integral form of the governing equations and preserve conservation laws by construction, are very popular in computational fluid dynamics.

Preserving conservation properties in a simulation method is also advantageous for simulations of incompressible turbulence. Turbulence forms a cascade of progressively smaller flow structures. In practice it is often not possible to capture the full range of turbulent flow structures on the computational grid. Once the size of the smallest flow structures in the solution approaches the mesh spacing, the dynamics of these flow structures can no longer be accurately predicted. General finite-volume methods

for general curvilinear grids allow under-resolved flow structures to generate kinetic energy, which may cause instability of the numerical simulation. For incompressible flow this instability can be eliminated by preserving conservation of kinetic energy by the convective term at the discrete level; see for example the discretizations proposed in [2] and [3]. These staggered discretizations of the incompressible Navier-Stokes equations eliminate the convective instability, and allow for stable simulations without ad hoc smoothing. This makes kinetic energy preserving discretizations very suitable for simulations of incompressible turbulence.

Simulations of compressible turbulent flow are also expected to benefit from kinetic energy conservation by the convective terms. Kinetic energy conserving discretizations have been proposed for both collocated curvilinear and staggered rectangular computational grids; see for example [4–6]. Kinetic energy conservation is related to the mathematical skew-symmetry of the convective terms, and therefore these discretizations are often called symmetry-preserving or skew-symmetric discretizations. Symmetry-preserving methods eliminate the convective nonlinear instability that plagues higher-order accurate simulations on general curvilinear grids, and allow for stable simulations of turbulence with low artificial dissipation. In an earlier paper, a fourth-order accurate symmetry-preserving discretization was applied to compressible channel flow [7]. It was shown that preserving the skew-symmetry of convective terms allows for simulations of subsonic channel flow without any artificial dissipation, and that the method is very suitable for large-eddy simulation (LES). In the present paper the method is applied to a more challenging external flow; the subsonic transitional flow over a delta wing.

GOVERNING EQUATIONS

The flow of air is modeled by the compressible Navier-Stokes equations. In conservative form the compressible Navier-Stokes equations read

$$\begin{aligned} \partial_t \rho + \nabla\cdot(\rho\vec{u}) &= 0 \\ \partial_t \rho\vec{u} + \nabla\cdot(\rho\vec{u}\vec{u}) + \nabla p &= \nabla\cdot\sigma \\ \partial_t \rho E + \nabla\cdot(\rho\vec{u}E) + \nabla\cdot(p\vec{u}) &= \nabla\cdot(\sigma\cdot\vec{u}) + \nabla\cdot\vec{q} \end{aligned} \tag{1}$$

where ρ is the mass density, $\vec{u}$ the flow velocity and E the total energy per unit mass. The conservative form of the compressible Navier-Stokes equations expresses conservation of mass, momentum and total energy in a fluid. The evolution equations for the total energy can be replaced by the evolution equation for the internal energy $e = E - \vec{u}\cdot\vec{u}/2$

$$\partial_t \rho e + \nabla\cdot(\rho\vec{u}e) + p\nabla\cdot\vec{u} = \sigma : \nabla\vec{u} + \nabla\cdot\vec{q} \tag{2}$$

The second terms in the left-hand-side of the above equations model transportation of a physical quantity with the flow velocity $\vec{u}$. These terms are called the convective terms in this paper.

To close the compressible Navier-Stokes equations, the dependence of the pressure p, viscous stress σ and diffusive heat flux $\vec{q}$ on the variables ρ, $\vec{u}$ and E (or e) should be specified. Air is assumed to be a callorically perfect gas $p = \rho RT$ where R is the gas constant and T the temperature which is assumed to be related to the internal energy through $T = e/c_v$. The viscous stress tensor σ is related to the strain tensor $S = (\nabla u + (\nabla u)^{\mathrm{T}})/2$ by the assumption of a Newtonian fluid

$$\sigma_{ij} = 2\mu(T)\left(S_{ij} - \frac{1}{3}\mathrm{tr}(S)\delta_{ij}\right) \tag{3}$$

where the dynamic viscosity is modeled by Sutherland's law

$$\mu(T) = \mu_\infty \left(\frac{T}{T_\infty}\right)^{\frac{3}{2}} \frac{T_\infty + T_{\mathrm{S}}}{T + T_{\mathrm{S}}} \tag{4}$$

with the constant T_{S} is set to 110.4 K. The heat diffusion is modeled through Fourier's law $\vec{q} = -\kappa\nabla T$.

The skew-symmetric nature of the convective terms

The convective transport terms conserve many physical global quantities. This conservation can be related to a mathematical skew-symmetry if the convective terms are rewritten to an alternative form. By preserving this skew-symmetry at the discrete level, many convective conservation properties can be transferred straightforwardly to the simulation method. In this section first the alternative form of the convective terms is defined, and second it is shown that this form is equivalent the convective terms from the conservative form of the Navier-Stokes equations.

The state of a compressible fluid is expressed in alternative square root variables $\sqrt{\rho}$, $\sqrt{\rho}\vec{u}$, $\sqrt{\rho e}$. The convective transport of these variables can be expressed as

$$\partial_t \phi + c(\vec{u})\phi = \ldots \tag{5}$$

where the ϕ denotes one of the above variables, the dots denote non-convective terms, and the convective operator is given by

$$c(\vec{u})\phi = \frac{1}{2}\nabla\cdot(\vec{u}\phi) + \frac{1}{2}\vec{u}\cdot\nabla\phi\,. \tag{6}$$

This operator is skew-symmetric, which means that

$$\psi c(\vec{u})\phi + \phi c(\vec{u})\psi = \nabla\cdot(\vec{u}\phi\psi) \tag{7}$$

is a divergence form. If the convective transport of ϕ and ψ satisfies Eqn. (5) then the product $\phi\psi$ satisfies

$$\partial_t(\phi\psi) = -\psi c(\vec{u})\phi - \phi c(\vec{u})\psi + \ldots = -\nabla\cdot(\vec{u}\phi\psi) + \ldots \quad (8)$$

so that $\phi\psi$ is conserved under convective transport by the skew-symmetry of $c(\vec{u})$. By substituting $\phi = \psi = \sqrt{\rho}$, $\phi = \sqrt{\rho}$ and $\psi = \sqrt{\rho}\vec{u}$, and $\phi = \psi = \sqrt{\rho e}$, the convective terms of the continuity, momentum, and internal energy equations are obtained. Thus, the form in Eqn. (5) is equivalent to the convective terms from the compressible Navier-Stokes equations.

The advantage of using the alternative form of the convective terms is that its skew-symmetry immediately implies that products of the variables $\sqrt{\rho}$, $\sqrt{\rho}\vec{u}$, and $\sqrt{\rho e}$ are conserved by convective transport. Thus skew-symmetry implies that the convective terms conserve mass, momentum, kinetic energy, internal energy, and so on. By preserving the skew-symmetry of the convective terms at the discrete level, a simulation method which mimics the many conservation properties of the convective terms is attained.

NUMERICAL METHOD

The numerical method used in this research combines a fourth-order accurate symmetry-preserving spatial discretization of the compressible Navier-Stokes equations with an explicit four-stage low-storage Runge-Kutta time-integration method. The most distinctive property of the numerical method is the symmetry-preserving spatial discretization. Whereas a general finite-volume discretization of the convective terms of the Navier-Stokes equations only conserves mass, momentum and total energy, a symmetry-preserving discretization of the convective terms also conserves the kinetic energy and internal energy separately. Preserving the kinetic energy conservation of the convective terms at the discrete level considerably improves the stability of a simulation method [7]. Therefore a symmetry-preserving discretization needs less artificial dissipation for stability than a general finite-volume discretization, which makes the symmetry-preserving discretization very suitable for simulations of turbulence and aero-acoustics.

Symmetry-preserving spatial discretization

A symmetry-preserving spatial discretization of the compressible Navier-Stokes equations transfers the conservation properties of the continuous compressible Navier-Stokes equation with respect to mass, momentum, kinetic energy, internal energy and total energy to the simulation method. The conservative form of the compressible Navier-Stokes equations in Eqn. (1) shows that all the terms conserve mass, momentum and total energy. This is naturally transferred to the discrete level by a finite-volume discretization. In the above it was shown that the convective transport does not only conserve mass, momentum an total energy, but also kinetic and internal energy separately. Therefore special attention is paid to the discretization of the convective terms.

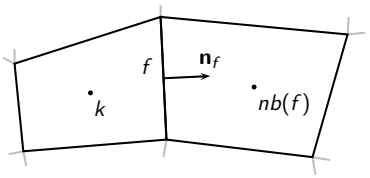

FIGURE 1. A GRID CELL K AND ITS NEIGHBOR.

Convective terms. To preserve the many conservation properties of the convective terms at the discrete level, the discretization of the convective operator given in Eqn (6) should be a skew-symmetric discrete operator. This means that a discrete counterpart of the Eqn. (7) should hold at the discrete level. A second-order accurate discretization of the convective term in grid cell k is

$$(c(\vec{u})\phi)_k = \frac{1}{\Omega_k}\sum_{f\in F_k}\frac{1}{2}A_f\vec{n}_f\cdot\vec{u}_f\phi_{nb(f)} \quad (9)$$

where F_k is the set of faces of cell k, A_f the area of face f, $\vec{n}_f$ a outward-pointing unit normal at face f, and $\vec{u}_f$ some interpolation of $\vec{u}$ to face f (see Fig. 1). This discretization is skew-symmetric because

$$\psi_k(c(\vec{u})\phi)_k + \phi_k(c(\vec{u})\psi)_k = \frac{1}{\Omega_k}\sum_{f\in F_k}A_f\vec{n}_f\cdot\vec{u}_f\widetilde{(\phi\psi)}_f \quad (10)$$

where $\widetilde{(\phi\psi)}_f = (\phi_k\psi_{nb(f)} + \phi_{nb(f)}\psi_k)/2$. This is a finite-volume discretization of Eqn. (7) because $A_f\vec{n}_f\cdot\vec{u}_f\widetilde{(\phi\psi)}_f$ is a flux function at face f, and therefore the proposed discretization conserves mass, momentum, kinetic energy and internal energy for ϕ equal to $\sqrt{\rho}$, $\sqrt{\rho}\vec{u}$, and $\sqrt{\rho e}$. More details of the symmetry-preserving discretization of the convective terms can be found in [7]. Assuming exact time integration and point-wise equalities of the form $(\phi^2)_k = (\phi_k)^2$, the above discretization can be rewritten to an induced finite-volume discretization of the convective terms

$$\partial_t\rho_k + \frac{1}{\Omega_k}\sum_{f\in F_k}A_f\vec{n}_f\cdot\vec{u}_f\widetilde{(\sqrt{\rho}\sqrt{\rho})}_f = 0 \quad (11)$$

$$\partial_t(\rho u_i)_k + \frac{1}{\Omega_k}\sum_{f\in F_k}A_f\vec{n}_f\cdot\vec{u}_f\widetilde{(\sqrt{\rho}\sqrt{\rho})}_f\overline{(u_i)}_f = \ldots$$

$$\partial_t(\rho E)_k + \frac{1}{\Omega_k}\sum_{f\in F_k}A_f\vec{n}_f\cdot\vec{u}_f\widetilde{(\sqrt{\rho}\sqrt{\rho})}_f\widetilde{E}_f = \ldots \quad (12)$$

where $\overline{\phi}_f = (\phi_k + \phi_{nb(f)})/2$ and $\widetilde{E}_f = (\widetilde{u_i u_i})_f/2 + (\widetilde{\sqrt{e}\sqrt{e}})_f$. By construction, this discretization of the convective terms conserves mass, momentum, kinetic energy, and internal energy. The discretization can be completed by specifying the interpolation $\vec{u}_f$, which is set to

$$\vec{u}_f = \frac{\overline{\rho}_f \overline{\vec{u}}_f}{(\widetilde{\sqrt{\rho}\sqrt{\rho}})_f} \tag{13}$$

so that most density square-roots cancel out of the finite-volume discretization.

A higher-order symmetry-preserving discretization can be constructed from the second-order accurate discretization derived above by Richardson extrapolation. For the convective terms, Richardson extrapolation is applied with three control volumes Δ, 2Δ and 3Δ as in [4]. The vertices of the 2Δ control volume, which do not coincide with vertices of the original grid, are approximated to fourth-order accuracy. The result is a symmetry-preserving fourth-order accurate discretization with a minimized dispersion error in computational space [8].

General central finite-volume discretizations of the convective terms allow for a convective transfer of internal energy to kinetic energy, and vice versa. If a curvilinear computational grid does not completely resolve the smallest turbulent flow structures, then general higher-order accurate finite-volume discretizations may predict a considerable transfer of internal energy to kinetic energy through the convective terms. This non-physical source of kinetic energy yields inappropriate results and can eventually cause numerical instability. Symmetry-preserving discretization of the convective terms does not allow the spurious transfer of internal to kinetic energy through the convective terms, and therefore eliminates such instabilities by construction. Indeed, symmetry-preserving discretization of the convective terms is observed to enhance the stability of a numerical method [4].

An important application area of the symmetry-preserving discretization is large-eddy simulation. In large-eddy simulation, the dissipation of resolved kinetic energy by sub-grid scales is modeled [9], and therefore the underlying discretization should not dissipate or generate kinetic energy. The symmetry-preserving discretization of convection conserves kinetic energy by construction, and thus the kinetic energy is only dissipated by the large-eddy simulation model. In a previous paper [7], it was shown that the symmetry-preserving discretization is a very suitable base discretization for large-eddy simulation of channel flow.

Pressure terms. The pressure terms conserve momentum and total energy, but do not conserve kinetic energy and internal energy separately. These conservation properties are captured appropriately by a finite-volume discretization. Here the second-order accurate product-rule preserving discretization proposed in [4] is used

$$\begin{aligned}(\nabla p)_k &= \frac{1}{\Omega_k} \sum_{f \in F_k} A_f \vec{n}_f \overline{p}_f \\ (\nabla \cdot (p\vec{u}))_k &= \frac{1}{\Omega_k} \sum_{f \in F_k} A_f \vec{n}_f \cdot \widetilde{(p\vec{u})}_f \end{aligned} \tag{14}$$

In the same way as for the convective terms, a fourth-order accurate dispersion-relation-preserving discretization of the pressure terms is constructed through Richardson extrapolation with three control volumes.

Viscous terms. The viscous terms conserve momentum and total energy. The viscous terms do not conserve kinetic energy and internal energy separately, but instead transfer kinetic energy into internal energy by viscous friction. In this paper a finite-volume discretization of the viscous terms is used. Again the base discretization is second-order accurate, and a fourth-order accurate discretization is derived using Richardson extrapolation with the two control volumes Δ and 2Δ. The second-order accurate base discretization is

$$\begin{aligned}(\nabla \cdot \sigma)_k &= \frac{1}{\Omega_k} \sum_{f \in F_k} A_f \vec{n}_f \cdot \sigma_f \\ (\nabla \cdot (\sigma \cdot \vec{u}))_k &= \frac{1}{\Omega_k} \sum_{f \in F_k} A_f \vec{n}_f \cdot \left(\sigma_f \cdot \frac{\overline{\rho u}_f}{\overline{\rho}_f} \right) \end{aligned} \tag{15}$$

The stress tensor σ_f at face f is computed using standard-finite difference discretization. Once again, in the computations with the 2Δ control volume the cell vertices are computed to fourth-order accuracy.

Heat transfer term. The heat transfer term only conserves total energy and internal energy. A general finite-volume method preserves these conservation properties. Once again, the base discretization of the heat transfer term is second-order accurate

$$(\nabla \cdot \vec{q})_k = \frac{1}{\Omega_k} \sum_{f \in F_k} A_f \vec{n}_f \cdot \vec{q}_f \tag{16}$$

where $\vec{q}_f$ is a finite-difference approximation. A fourth-order accurate approximation is constructed using Richardson extrapolation with Δ and 2Δ control volumes to construct a fourth-order accurate discretization.

Time integration

Assuming exact time integration, the symmetry-preserving spatial discretization transfers conservation of mass, momentum, kinetic energy, internal energy and total energy to the simulation method. However, in practice errors due to numerical time integration can introduce considerable conservation errors, thereby canceling the numerical and physical advantages of using a symmetry-preserving spatial discretization.

It can be shown that so-called symplectic Runge-Kutta time-integration methods preserve the conservation properties of mass, momentum, kinetic energy and internal energy at the discrete level [7]. However, symplectic Runge-Kutta methods are implicit, and rigorous solution of the corresponding implicit system is required to obtain accurate conservation. An alternative is to use a general time-integration method with a sufficiently small time step size to control the conservation errors [10]. The latter approach is taken in this research; time integration is performed using a four-stage low-storage Runge-Kutta method, and the Courant number is set to 1 for stability and accuracy.

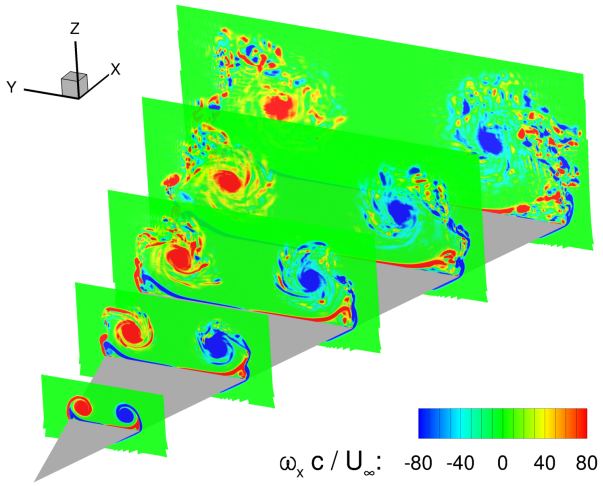

FIGURE 2. CONTOUR PLOTS OF THE AXIAL VORTICITY AT THE STATIONS X = 0.2 C, 0.4 C, 0.6 C, 0.8 C AND 1.0 C.

SIMULATION SETUP

To assess the stability and accuracy of the fourth-order accurate symmetry-preserving discretization, simulations of the flow over a sharp-edged delta wing at chord Reynolds number 50,000 are performed. The delta wing is similar to the wing studied by Visbal and Gordnier [11]; The angle of attack is 25°, and the sweep of the wing is 75°. However, in this paper the flow around a finite wing with a blunt trailing edge at Mach 0.3 is considered, whereas Visbal and Gordnier study the span wise symmetric flow around a semi-infinite wing at Mach 0.1. The bevel of the delta wing considered here is 30°.

The flow over a sharp-edged delta wing is dominated by a shear layer that originates at the leading edge. The shear layer rolls up into a marked conical flow structure which is called the primary vortex (see Fig. 2). At the considered Reynolds number, downstream from approximately 0.25 chord lengths the boundary layer on the upper surface of the delta wing separates and is partly sucked into the primary vortex. This creates a mixture of counter-rotating vortical substructures (sub-vortices) along the edge of the primary vortex.

From experimental measurements it is known that the time-averaged axial vorticity field above a delta wing features a captivating helical pattern [12, 13]. Numerical simulations by Visbal and Gordnier [11] suggest that this helical pattern is caused by a regular hydrodynamic transition process of the sub-vortices that are sucked into the primary vortex. For an infinite delta wing at chord Reynolds number 50,000, the helical pattern of sub-vortices has been observed downstream from approximately 0.6 chord lengths [11].

The surface of the delta wing is modeled as an isothermal no-slip boundary. The delta wing is positioned at the center of a computational domain that spans approximately 20 chord lengths in each direction. The computational domain is divided into a region of interest and a far field. The region of interest contains the delta wing and the primary vortex above the delta wing. The region of interest is a box of dimensions $[-0.04c, 1.06c] \times [-0.31c, 0.31c] \times [-0.04c, 0.27c]$ where the origin of the coordinate system is located at the apex of the delta wing, and c is the chord length of the delta wing. The purpose of the region of interest is to accurately capture the turbulent flow over the delta wing, and therefore the computational grid in this region is fine and smooth.

The purpose of the far field is to provide a natural transition from the region of interest to the boundaries of the computational domain. In the far field only the large flow structures are captured. Therefore the grid cell size in the far field increases towards the domain boundaries, and sixth-order artificial dissipation is applied to suppress spurious oscillations. At the inflow and outflow boundaries of the computational domain, characteristic boundary conditions are applied.

The computational grid is multi-block structured and curvilinear. The grid has a conical structure above the wing, so that the grid resolution relative to the size of the primary vortex is approximately constant in the tangential and span wise directions. Simulations are performed on a fine grid A of 27 million grid cells and a coarser grid B of 3.4 million grid cells. The fine grid A practically resolves the laminar boundary layer on the upper surface of the delta wing ($\Delta x^+_{max} \approx 22$, $\Delta y^+_{max} \approx 16$, $\Delta z^+_{min} \approx 1$, $\Delta z_{min}/c = 1.7 \times 10^{-4}$). In the primary vortex the fine grid resembles the finest computational grid used in [11]. The coarser grid B is two times as coarse as the fine grid; the mesh spacing is doubled with respect to the fine grid A. Table 1 lists the grid

TABLE 1. DIMENSIONS OF THE LARGEST CELLS AT THE TRAILING EDGE OF THE DELTA WING.

Grid	Cells	$\Delta x/c$	$\Delta y/c$	$\Delta z/c$
A	2.7×10^{7}	4.6×10^{-3}	3.4×10^{-3}	3.0×10^{-3}
B	3.4×10^{6}	9.2×10^{-3}	6.8×10^{-3}	6.0×10^{-3}

resolution in the vortex core for both grids.

The initial condition of the simulations is an unsteady RaNS solution of the delta wing flow. The dimensionless time step size is $\Delta tU_\infty/c = 7.5\times10^{-6}$ for the fine grid A and $\Delta tU_\infty/c = 1.5\times10^{-5}$ for the coarser grid B. The total simulation times on the grids A and B are 15 and 20 dimensionless time units. After approximately 2 dimensionless time units, on both grids the primary vortex has undergone transition to turbulence, and recording of flow statistics starts.

The simulations by Visbal and Gordnier [11] suggest that the coarser grid B does not resolve the turbulent flow above the delta wing. Therefore, a simulation on grid B with the symmetry-preserving discretization can be seen as an implicit large-eddy simulation. To provide some context for the results of this implicit large-eddy simulation, on the coarser grid also simulations are performed with the Vreman [14] and singular value [15] large-eddy simulation (LES) models, and with sixth-order artificial dissipation at the low level $k^{(6)} = 1/8$ [10]. For consistency, the LES models are discretized to fourth-order accuracy, just like the numerical discretization.

RESULTS AND DISCUSSION

Simulation with the symmetry-preserving discretization have been performed on the fine grid A and the coarser grid B. The symmetry-preserving discretization eliminates the nonlinear convective instability, so that little artificial dissipation is needed for numerical stability. In fact, the simulations on both the fine and the coarser grid are stable without any artificial dissipation in the region of interest, even though the simulation method is fourth-order accurate and the grid bends and stretches considerably. Figure 2 shows the flow field computed without artificial dissipation on the fine grid.

Figure 3 and Fig. 4 show contour plots of the instantaneous axial vorticity at the location $x/c = 0.5$ computed on the fine grid A and the coarser grid B without LES model or artificial dissipation. Separation of the laminar boundary layer on the upper surface of the delta wing and the suction of sub-vortices into the primary vortex is observed on both the grids. Due to the absence of modeled or artificial dissipation, mild spurious oscillations can be observed in the axial vorticity fields. For general

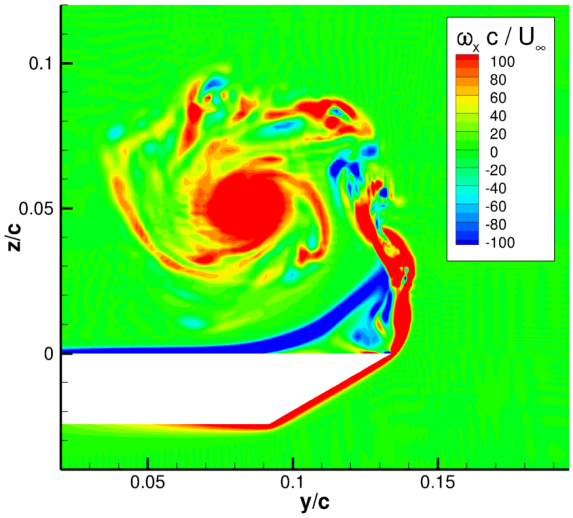

FIGURE 3. THE INSTANTANEOUS AXIAL VORTICITY AT X/C = 0.5 COMPUTED ON THE FINE GRID A.

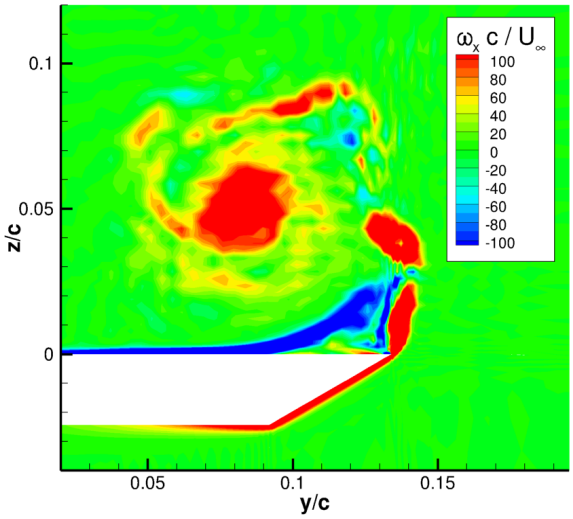

FIGURE 4. THE INSTANTANEOUS AXIAL VORTICITY AT X/C = 0.5 COMPUTED ON THE COARSER GRID B.

finite-volume methods spurious oscillations can trigger the nonlinear convective instability, and typically modeled or artificial dissipation is needed to stabilize simulations. For a symmetry-preserving method mild spurious oscillations cannot cause numerical instability through convective transport, and the simulations are stable without artificial dissipation in the region of interest. For the current simulations the application of artificial dissipation is a modeling choice, and not a necessary condition for numerical stability.

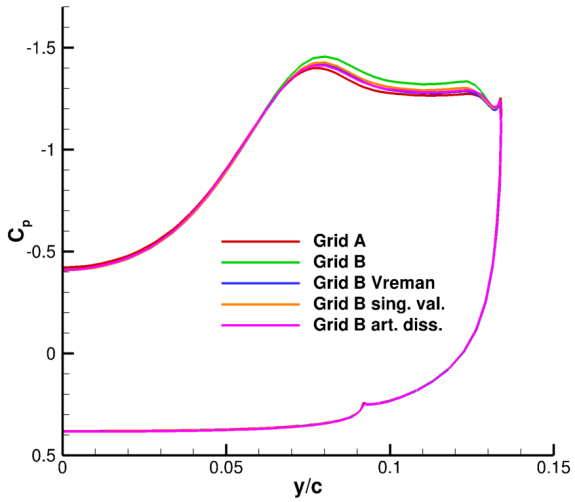

FIGURE 5. THE MEAN PRESSURE COEFFICIENT AT X/C = 0.5.

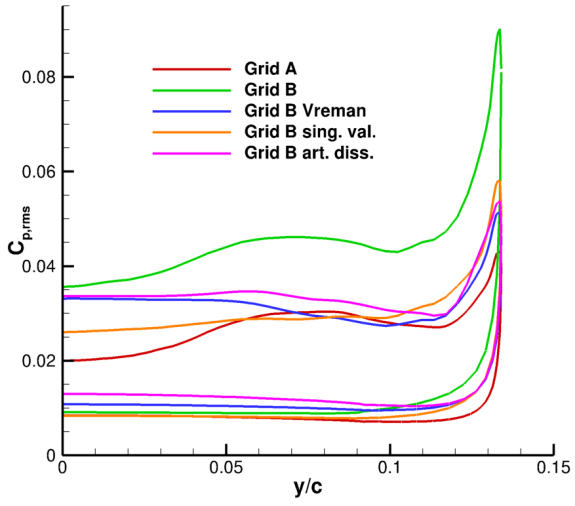

FIGURE 6. FLUCTUATIONS OF THE PRESSURE COEFFICIENT AT X/C = 0.5.

Figure 5 shows the mean pressure coefficient C_p on the surface of the delta wing at $x/c = 0.5$. The simulations without LES model or artificial dissipation on the fine grid A and the coarser grid B predict similar mean pressures over most of the delta wing surface. Small differences are observed underneath the primary vortex, where the fine grid simulation predicts a higher pressure than the simulation on the coarser grid. Simulations on the coarser grid with the Vreman and singular value LES model and with sixth-order artificial dissipation predict pressures in between the levels predicted by the simulations on the fine and the coarser grid without LES model or artificial dissipation.

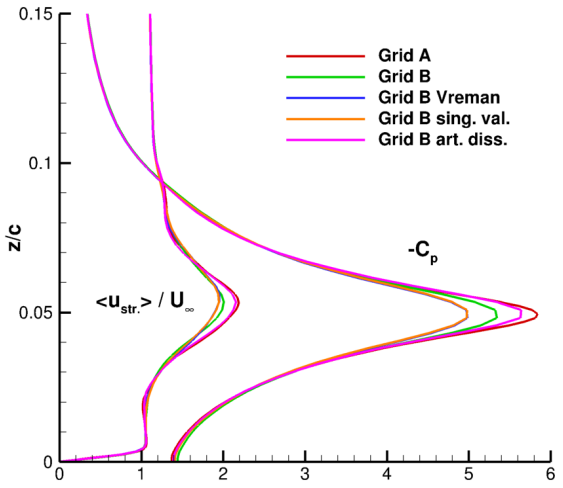

FIGURE 7. THE MEAN STREAM WISE FLOW VELOCITY AND THE (NEGATIVE) PRESSURE COEFFICIENT ON A LINE THROUGH THE VORTEX CORE AT X/C = 0.5. THE PREDICTIONS OBTAINED WITH THE VREMAN AND SINGULAR VALUE LES MODELS COLLAPSE.

The root mean square of the pressure coefficient fluctuations on the surface of the delta wing at $x/c = 0.5$ is shown in Fig. 6. The coarser grid B does not resolve the boundary layer on the upper surface of the delta wing, and the simulation without an LES model or artificial dissipation on the coarser grid over-predicts the pressure fluctuations on the upper surface of the delta wing. This corroborates an observation in an earlier paper [7], where it was shown that the symmetry-preserving discretization typically over-predicts fluctuations in under-resolved simulations of compressible turbulent channel flow. Application of an LES model or sixth-order artificial dissipation reduces the fluctuations of the pressure coefficient to levels predicted by a simulation on the fine grid A.

Figure 7 shows the mean pressure coefficient and the mean stream wise velocity on a vertical line through the laminar vortex core at $x/c = 0.5$ and $y/c = 0.084$. The simulations on the fine and the coarser grid both predict a suction peak and a local maximum of the stream wise velocity at $z/c = 0.05$, where the center of the vortex core is located (cf. Fig. 3). The simulation on the fine grid A predict a suction peak of strength $C_p = -6.0$. The coarser grid B does not resolve the vortex core, and predicts a weaker suction peak. Application of the Vreman or singular value LES model on the coarser grid B weakens the strength of the suction peak further. However, application of sixth-order artificial dissipation on the coarser grid B strengthens the suction peak, and predicts a suction close to the suction computed on the fine grid. The mean stream wise velocity in the laminar vortex core exhibits a similar qualitative behavior; the symmetry-preserving method predicts a lower mean flow velocity on the

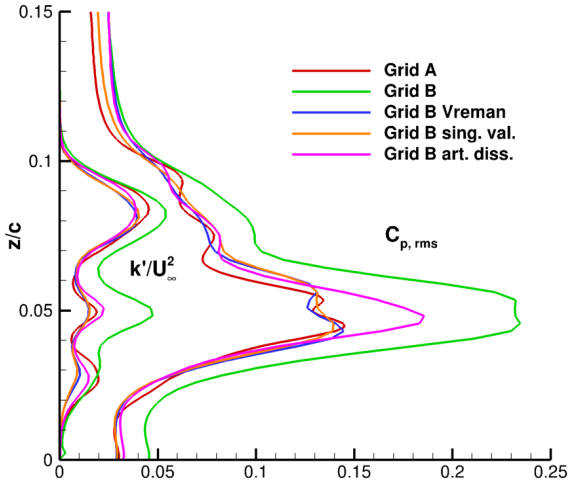

FIGURE 8. THE RESOLVED TURBULENT KINETIC ENERGY AND THE PRESSURE COEFFICIENT FLUCTUATIONS ON A LINE THROUGH THE VORTEX CORE X/C = 0.5.

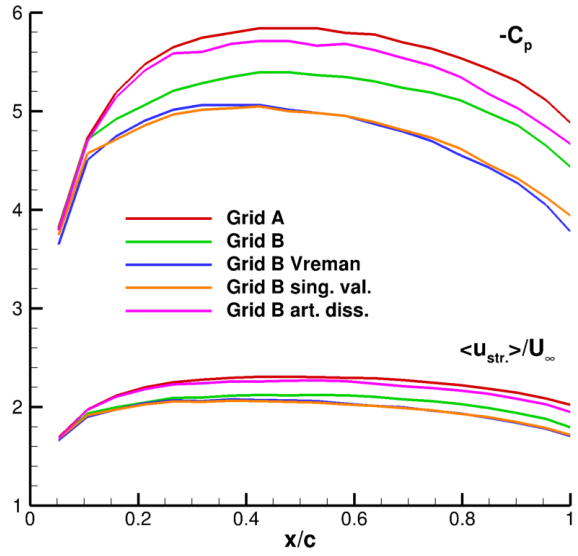

FIGURE 9. THE PRESSURE COEFFICIENT AND THE STREAM WISE VELOCITY IN THE THE VORTEX CORE.

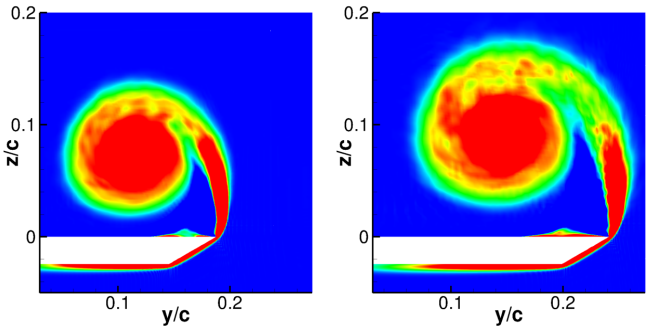

FIGURE 10. THE MEAN AXIAL VORTICITY AT THE STATIONS X/C = 0.7 AND X/C = 0.9.

coarser grid than on the fine grid, the application of an LES model lowers the flow velocity further, and the application of sixth-order artificial dissipation increases the flow velocity towards the flow velocity predicted on the fine grid.

Figure 8 shows the resolved turbulent kinetic energy k'/U_∞^2 and the root mean square of the pressure coefficient fluctuations along the same vertical line at $x/c = 0.5$ and $y/c = 0.084$. The resolved turbulent kinetic energy attains a local maximum in the vortex core at $z/c = 0.05$, but also at $z/c = 0.03$ and $z/c = 0.08$, where the turbulent shear layer crosses the vertical line (cf. Fig. 3). Just like along the surface of the delta wing, on the coarser grid B the simulation without LES model or artificial dissipation over-predicts fluctuations in the under-resolved vortex core. The application of an LES model or sixth-order artificial dissipation on the coarser grid reduces the turbulent fluctuations to levels predicted on the fine grid.

Figure 9 shows the mean pressure coefficient and the mean stream wise velocity at the center of the vortex core as a function of the axial location x/c. These quantities peak approximately in the middle of the delta wing, and decrease towards the trailing edge. The qualitative behavior at $x/c = 0.5$ observed in Fig. 7 holds throughout the vortex core; at all the axial locations the simulation on the fine grid A predicts the strongest suction peak and the highest stream wise flow velocity, and the simulation on the coarser grid B with LES model predicts the weakest suction peak and the lowest stream wise flow velocity. Throughout the vortex core, the simulation on the coarser grid with sixth-order artificial dissipation predicts a stronger suction peak and higher mean stream wise flow velocity than the implicit large-eddy simulation on the coarser grid.

Simulations of the span wise symmetric flow over an infinite delta wing at chord Reynolds number 50,000 by Visbal and Gordnier [11] predict a mean stream wise velocity of 4.0 in the vortex core at $x/c = 1.0$. Figure 9 shows that the simulation of a finite delta wing on the fine grid A predicts a mean stream wise velocity of 2.0 in the vortex core at $x/c = 1.0$, and a maximum mean stream wise velocity of 2.3 at $x/c = 0.45$. The marked difference between the prediction in [11] and the simulation on the fine grid A is most likely due to the wake at the trailing edge of the finite delta wing considered here. The wake at the trailing edge imposes a boundary condition on the flow above the delta wing which is fundamentally different from the infinity boundary condition imposed in [11]. Different boundary conditions correspond to different primary vortices, and to different flow velocities in the vortex core.

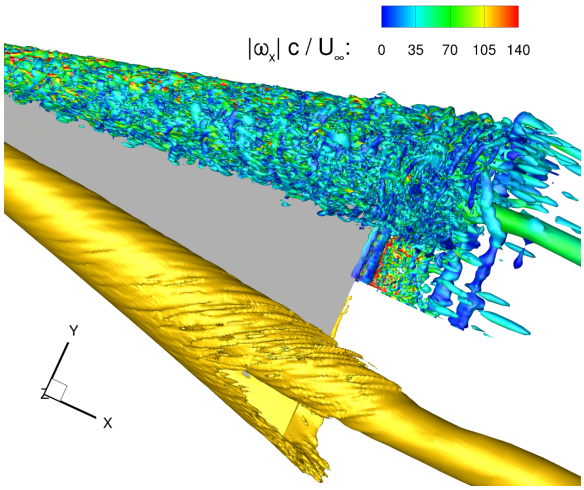

FIGURE 11. AN ISOSURFACE OF THE INSTANTANEOUS Q-CRITERION COLORED BY THE INSTANTANEOUS AXIAL VORTICITY (TOP) AND AN ISOSURFACE OF THE MEAN AXIAL VORTICITY (BOTTOM).

The time-averaged axial vorticity field on the fine grid recorded over 13 dimensionless time units features sub-vortices downstream from approximately $x/c = 0.5$. By tracing the sub-vortices through contour plots at different axial locations, the sub-vortices are observed to rotate around the vortex core in helical trajectories. Figure 10 shows contour plots of the mean axial vorticity at $x/c = 0.7$ and $x/c = 0.9$. The observed sub-vortices are not as pronounced as in experimental measurements [12, 13], possibly because the current chord Reynolds number is considerably lower than in the experiments, because the time-averages are not converged sufficiently, or because the computational grid is not fine enough.

The numerical simulations by Visbal and Gordnier [11] predicts mean sub-vortices of constant magnitude over a large range of axial locations. Therefore an iso-surface of the mean axial vorticity shows long helical trajectories described by the mean sub-vortices. The current simulations of a finite delta wing on the fine grid predict mean sub-vortices of a magnitude that decreases towards the trailing edge of the delta wing. Figure 11 shows the iso-surface $< \omega_x > c/U_\infty = -14$ computed over 13 dimensionless time units on the fine grid A. The iso-surface shows helical trajectories, but only over limited range of axial locations. The iso-surfaces shown in [11] and here can be different because the flow over an infinite wing is fundamentally different from the flow over a finite wing, because the time-averages are recorded over time intervals of different length, or because the grid resolutions are slightly different.

The mean sub-vortices computed on the fine grid A describe helical trajectories, but are not very pronounced. To ensure that the mean sub-vortices computed in the current simulations are indeed similar to the mean sub-vortices observed in other experimental and numerical studies [11–13], time-averages over longer time intervals should be computed.

CONCLUSION

Simulations of the flow over a sharp-edged delta wing have been performed with a fourth-order accurate symmetry-preserving discretization for compressible flow. A symmetry-preserving discretization of the convective terms preserves conservation of kinetic energy at the discrete level, and thereby improves the numerical stability of a simulation method. Indeed, although general finite-volume methods are typically unstable unless artificial dissipation is applied, the current simulations are stable without modeled or artificial dissipation in a region of interest around the delta wing. Thus, for these simulations the application of modeled or artificial dissipation is optional, and not a necessary condition for numerical stability.

Simulations have been performed on a fine and a coarser computational grid. Results of simulations on the coarser grid with large-eddy simulation (LES) models, with sixth-order artificial dissipation, and simulations on the coarser grid without modeled or artificial dissipation have been compared with the results of a fine grid simulation. In the vortex core, the simulation on the coarser grid without modeled or artificial dissipation predicts a weaker suction peak and higher turbulent fluctuations in the vortex core than the simulation on the fine grid. Application of an LES model on the coarser grid weakens the suction peak further, but correctly reduces the turbulent fluctuations. Application of sixth-order artificial dissipation on the coarser grid strengthens the suction peak to a level that approaches the fine grid result, and also correctly reduces the turbulent fluctuations.

The time-averaged axial vorticity field computed on the fine grid features sub-vortices that rotate around the vortex core in helical trajectories. Further research is needed to investigate whether these mean sub-vortices are similar to the mean sub-vortices that have been observed in other experimental and numerical studies.

ACKNOWLEDGMENT

This research is funded by the Ubbo Emmius Fund of the University of Groningen. We thank the National Aerospace Laboratory NLR for supporting this research.

REFERENCES

[1] LeVeque, R. J., 2002. *Finite Volume Methods for Hyperbolic Problems*. Cambridge University Press, New York, NY.

[2] Morinishi, Y., Lund, T. S., Vasilyev, O. V., and Moin, P., 1998. "Fully Conservative Higher Order Finite Difference Schemes for Incompressible Flow". *J. Comput. Phys.,* ***143***, pp. 90–124.

[3] Verstappen, R. W. C. P., and Veldman, A. E. P., 2003. "Symmetry-preserving discretization of turbulent flow". *J. Comput. Phys.,* ***187***, pp. 343–368.

[4] Kok, J. C., 2009. "A high-order low-dispersion symmetry-preserving finite-volume method for compressible flow on curvilinear grids". *J. Comput. Phys.,* ***228***, pp. 6811–6832.

[5] Subbareddy, P. K., and Candler, G. V., 2009. "A fully discrete, kinetic energy consistent finite-volume scheme for compressible flows". *J. Comput. Phys.,* ***228***, pp. 1347–1364.

[6] Morinishi, Y., 2010. "Skew-symmetric form of convective terms and fully conservative finite difference schemes for variable density low-Mach number flows". *J. Comput. Phys.,* ***229***, pp. 276–300.

[7] Rozema, W., Kok, J. C., Verstappen, R. W. C. P., and Veldman, A. E. P., 2014. "A symmetry-preserving discretization and regularization model for compressible flow with application to turbulent channel flow". *J. Turbul.* submitted.

[8] Tam, C. K. W., and Webb, J. C., 1993. "Dispersion-Relation-Preserving Finite Difference Schemes for Computational Acoustics". *J. Comput. Phys.,* ***107***, pp. 262–281.

[9] Garnier, E., Adams, N., and Sagaut, P., 2009. *Large Eddy Simulation for Compressible Flows*. Springer.

[10] Kok, J. C., and Van der Ven, H., 2012. Capturing free shear layers in hybrid RANS-LES simulations of separated flow. Tech. Rep. NLR-TP-2012-333, National Aerospace Laboratory NLR. See also URL `http://hdl.handle.net/10921/914`.

[11] Visbal, M. R., and Gordnier, R. E., 2003. "On the Structure of the Shear Layer Emanating from a Swept Leading Edge at Angle of Attack". In Proc. 33rd AIAA Fluid Dynamics Conference and Exhibit. AIAA 2003-4016.

[12] Riley, A. J., and Lowson, M. V., 1998. "Development of a three-dimensional free shear layer". *J. Fluid Mech.,* ***369***, pp. 49–89.

[13] Mitchell, A. M., Morton, S. A., Forsythe, J. R., and Cummings, R. M., 2006. "Analysis of Delta-Wing Vortical Substructures Using Detached-Eddy Simulation". *AIAA J.,* ***44***, pp. 964–972.

[14] Vreman, A. W., 2004. "An eddy-viscosity subgrid-scale model for turbulent shear flow: Algebraic theory and applications". *Phys. Fluids,* ***16***, pp. 3670–3681.

[15] Nicoud, F., Toda, H. B., Cabrit, O., Bose, S., and Lee, J., 2011. "Using singular values to build a subgrid-scale model for large eddy simulations". *Phys. Fluids,* ***23***, p. 085106.